Research Square

Preprints are preliminary reports that have not undergone peer review.
They should not be considered conclusive, used to inform clinical practice,
or referenced by the media as validated information.

Early hyperspectral detection of Carlavirus vignae in common bean under field conditions

William Rafael Ribeiro
José Francisco Arruda Silva
Andressa de Souza Almeida
Amanda Lopes Ferreira
Rômulo Moreira Silva
Tavvs Micael Alves
Alaerson Maia Geraldine
Patrícia Valle Pinheiro
Murillo Lobo Junior
murillo.lobo@embrapa.br

Empresa Brasileira De Pesquisa Agropecuária https://orcid.org/0000-0002-3681-4570

Research Article

Keywords: Plant spectral response, Phaseolus vulgaris, precision agriculture, phytopathometry, remote sensing

Posted Date: June 9th, 2026

DOI: https://doi.org/10.21203/rs.3.rs-9694653/v1

License: This work is licensed under a Creative Commons Attribution 4.0 International License. Read Full License

Abstract

Virus-associated diseases are among the biological stresses that affect common bean yield, such as *Carlavirus vignae* (*Cowpea mild mottle virus*, CPMMV), transmitted by the whitefly *Bemisia tabaci*. CPMMV is present in different continents, and recent outbreaks have concerned Brazilian farmers and researchers. Integrated Pest Management routines for field monitoring of viral spread are laborious and may be limited to visible symptoms. We hypothesized that CPMMV infection can be detected in asymptomatic plants by differences in the plant canopy reflectance. To test this hypothesis, we used a hyperspectral sensor mounted on a drone to capture images of CPMMV-inoculated and non-inoculated field plots in 2022 and 2023, across a tolerant common bean cultivar (BRS FC420 RMD) and a susceptible one (BRS FC401 RMD). Results showed that CPMMV was detected in common bean plants by hyperspectral imaging at early infection stages (~ 6 DAI) before symptom onset and at an advanced infection stage (~ 22 DAI). Reflectance within the visible light spectrum was affected by soil cover on all flights, and in most of these, also in the near-infrared region. The main differences between CPMMV-inoculated and control plants were consistent across two years of experiments, regardless of the common bean phenological stage and genotype. Fit statistics using the sum of squared errors, R^2 and AIC indicated that reflectance from 401 to 425 nm, especially near 415 nm, differed significantly between infected and healthy plants. Such changes are associated with chlorophyll degradation and disruption of the photosynthetic apparatus, and are detectable even before symptom onset. Progress in the disease severity index also differentiated the tolerant cultivar from the susceptible one. CPMMV infection significantly reduced common bean yield by ~ 21% compared with healthy plants. CPMMV detection by hyperspectral imaging enables early scouting to optimize disease management.

Introduction

Common beans (*Phaseolus vulgaris* L.) are widely cultivated for their nutritional value and are a staple food in Latin America and African countries. In South America, *Carlavirus vignae* (Cowpea mild mottle virus, CPMMV) and *Begomovirus costai* (formerly Bean golden mosaic virus, BGMV) transmitted by the whitefly *Bemisia tabaci*, are major threats (Faria et al. 2016; Lamas et al. 2017). Extensive field testing has revealed that CPMMV outbreaks and mixed viral infections have become a concern in Brazil in recent years.

Virus-disease management in common beans relies mostly on synthetic insecticides aimed at the insect vector (Ferreira et al., 2024). Economic Injury Level is indeterminate and depends on the presence of the virus, which can spread rapidly even at low levels. Virus identification typically occurs when plants show symptoms, using visual monitoring or, if inconclusive, laboratory diagnostics, which are time-consuming and expensive.

Periodic field monitoring to identify pests and diseases is part of the Integrated Pest Management (IPM) protocols, but manual crop monitoring is labor-intensive and limits widespread adoption (Ferreira et al., 2025). Remote sensing offers a promising alternative for automated monitoring, streamlining disease detection and decision-making to prevent yield losses. Modern remote sensing tools, integrated with image-processing algorithms, enable fast, precise disease scouting over large areas (Bock et al., 2020).

Remote sensing can speed up diagnosis and management decisions for preventing the spread of plant diseases. Sensors that measure red, green, blue, and near-infrared light (i.e., electromagnetic energy) can be attached to drones to detect spectral changes in plants before symptoms are visible (Alves et al., 2015; Mahlein, 2016; Mahlein et al., 2018). Spectral responses are associated with early plant injury, including changes in chlorophyll content and photosynthetic activity (Zhang et al., 2019; Terentev et al., 2022). These responses can also be used to derive vegetation indices such as the Normalized Difference Vegetation Index (NDVI). These indices help distinguish healthy from sick plants and estimate disease severity or the number of infected plants in a field (Devadas et al., 2009). Hyperspectral sensors, which capture narrower spectral ranges, may detect more subtle plant responses and improve early disease detection. Flight routines

with automated imaging also let users quickly check large areas, cut manual monitoring costs, and advise pesticide use, addressing IPM gaps.

We hypothesized that CPMMV infection induces specific physiological responses in common bean plants that hyperspectral sensors can indirectly detect. Despite progress in hardware and methodologies for analyzing spectral data measured by remote sensors, their use for disease monitoring remains incipient. Successful cases in this context have been reported using a hyperspectral sensor to identify early and late blight in potatoes (Gold et al., 2020) and virus diseases in maize and grapes (Luo et al., 2021; Nguyen et al., 2021). To our knowledge, there are no reports of hyperspectral images for detecting common bean diseases. To test this, we conducted a field study using hyperspectral imaging to diagnose CPMMV. The objectives of this study were: 1) to evaluate the effectiveness of a hyperspectral sensor in the diagnosis of CPMMV in two different common bean genotypes, comparing healthy and inoculated plants; 2) to investigate whether the presence or absence of soil cover with mulch can influence the definition of hyperspectral signatures for infection in different bean genotypes; and 3) to quantify the potential yield losses related to CPMMV infection in the common bean crop.

Materials and Methods

Experimental design

A two-year (2022 and 2023) field experiment was conducted at Embrapa Rice and Beans in Santo Antônio de Goiás, Brazil (16º28'00"S, 49º17'00"W, 823m altitude), under center-pivot irrigation. The tropical Aw climate features distinct wet (October–April) and dry (May–September) seasons. We used a randomized block design with five replications per treatment in a 2 × 2 × 2 factorial: (i) BRS FC401 RMD or BRS FC420 RMD common bean cultivars, (ii) virus- or non-inoculated plants, and (iii) mulched or bare plots, since soil exposure may affect canopy spectral responses at early vegetative stages. Therefore, any variation observed in the imagery could reflect potential confounding effects that should be considered in the interpretation.

Both common bean cultivars (BRS FC401 RMD and BRS FC420 RMD) were developed by Embrapa (Faria et al 2016; Silva et al 2022). They belong to the Mesoamerican gene pool and exhibit the carioca grain type (beige with brown stripes), which accounts for approximately 70% of bean consumption in Brazil. These transgenic cultivars were developed using RNA interference (RNAi) and carry the RMD trait, which confers resistance to BGMV (Faria et al., 2016). Notably, BRS FC401 RMD is susceptible to CPMMV, whereas BRS FC420 RMD is tolerant, exhibiting mild or no symptoms (Silva et al., 2022).

CPMMV inoculum source

Symptomatic common bean leaf samples infected with the CPMMV isolate BR: GO:14 (GenBank MK202583) (Alves-Freitas et al., 2019) were used as the inoculum source. To confirm the viral infection, total RNA was extracted from CPMMV-infected common bean leaves using the Trizol protocol, as recommended by the manufacturer (Thermofisher), following cDNA synthesis, using the First-strand cDNA synthesis kit (Thermofisher) and oligodT primers. After quantification of the cDNA integrity and quality, PCR was performed using CPMMV primers (F:AACTTGGCCTTAGTGAACTCTACA/R: ATTAGCTCTGTGCCTGGGGT) that amplify a fragment of 500pb, from the coat protein CPMMV gene (Lamas et al 2017).

Crop management

The experiments were conducted in the same field over two consecutive years (2022 and 2023) under dry-season conditions, characterized by minimal rainfall and with center-pivot irrigation. The experiments were sown on May 27 2022, and on May 19, 2023. In both years, the irrigated field was cultivated in the previous cropping season with Congo grass

(*Urochloa ruziziensis*), which was terminated with glyphosate (2.0 kg ha^{-1}) followed by flail shredding two weeks before the experiment was implemented. Common bean seeds were treated to avoid eventual damage by soilborne pathogens and natural infestation of whiteflies, guaranteeing crop stand, with a fungicide/insecticide preparation (400 mL 100 kg^{-1}) of Fludioxonil (2.5%), Metalaxil-M (2.0 %), Thiabendazole (15.0%) and Thiamethoxam (35.0%) (Syngenta, Brazil). No-tillage sowing was carried out in the 20 plots of 60 m² each (10 m × 6 m). To ensure better reflectance capture and minimize interference from wide between-row spacing during the early plant stages, we reduced the standard row spacing from 50 cm to 25 cm while maintaining the regional recommendation of 20 plants m^{-2}.

Congo grass mulch was manually removed from plots assigned to the no–soil–cover treatment to ensure bare-soil conditions. In both years, monoammonium phosphate (12-61-00, 200 kg ha^{-1}) was the basal fertilizer applied at sowing. Seedling emergence began five days after planting in both years. Supplementary fertilization was applied 29 days after emergence (DAE), consisting of 30 kg ha^{-1} of KCl and nitrogen topdressing with urea at 200 kg ha^{-1}. Light and homogeneous infestations of the cucurbit beetle (*Diabrotica speciosa*) and ants (*Atta* spp.) were effectively controlled by insecticide spraying of fipronil (80% a. i.; BASF S.A., Brazil) at 100 g a.i. ha^{-1} + thiamethoxam (75% a. i., Syngenta) at 125 mL a.i. ha^{-1}). At the V3 stage, Fomesafen (25% a. i., UPL Open Ag) at 1.0 L ha^{-1} and Fluazifop-P-Butyl (25% a. i., Syngenta) at 1.0 L ha^{-1} were applied in all plots for weed management in 2022 and 2023.

Mechanical inoculation of CPMMV

In both years, plants were mechanically inoculated at 7 DAE (V2 stage with the primary leaves fully expanded) in the field. All plants in a 9 m² area (3 m × 3 m) in the center of each 60 m² plot were individually inoculated with CPMMV inoculum obtained from BRS FC401 RMD plants kept in a greenhouse (with viral infection previously confirmed by RT-PCR). CPMMV-infected leaves were crushed and homogenized in a blender with sodium phosphate buffer at pH 7.4 and sodium sulfite 0.01 M. In each 9 m^2 area, primary leaves were thoroughly rubbed with a gauze soaked in an inoculum suspension and carborundum abrasive (400 mesh). Control plots were not inoculated with CPMMV. The infection in the experimental plots was checked twice, at V3 and V4 (12 and 34 days after inoculation, DAI). For that, bulk leaf samples from 10 plants per plot were analyzed by RT-PCR to confirm the presence/absence of the virus in the plots. During 2022 and 2023, whiteflies were not detected in the experiments.

Disease severity rating

Disease severity assessments were initiated at the V3 plant stage (12 DAI) on 12 randomly selected plants in the 9 m² central area of each plot, using a 1-4 severity scale adapted from Silva et al. (2024). On our adapted scale, 1 equals all plants asymptomatic, 2 = mild chlorosis and mosaic symptoms, 3 = more severe chlorosis and/or mottling and vein clearing and 4 = severe leaf deformation, mottling, severe leaf crinkling, mostly in association with vein clearing, mosaic chlorosis and very pronounced wrinkling, causing reduced plant growth and development. Further, we estimated the disease severity index (DSI), a percentage-based measure derived from ordinal severity scale data (Chiang et al., 2017). The severity assessments were repeated at 6 or 7-day intervals Furthermore, the DSI results were checked for normality of residuals and heteroscedasticity using the Kolmogorov-Smirnov and Levene's tests, respectively, to adjust DSI progress curves by linear regression.

Crop yield

Plants at the R9 physiological maturity stage were desiccated with the herbicide Diquat at 2.0 L ha^{-1}(20% a. i.; Syngenta Proteção de Cultivos, Brazil) plus the adjuvant soybean oil methyl ester (0.4 L ha^{-1}, Agro Bayer, Brazil) to facilitate manual harvest on Sep 8, 2022, and Aug 23, 2023. Previously, 10 plants were randomly collected from a 9 m^2 area to estimate the weight of 100 grains. The remaining plants in the plot were manually harvested and then mechanically threshed. The grains were weighed, and after adjusting the moisture content to 13% (Figure 4D), productivity (kg ha^{-1}) was estimated. To

verify the assumptions of normality of the residuals and homoscedasticity, the Shapiro-Wilk and Bartlett tests were applied, respectively. All response variables met the assumptions and were subjected to analysis of variance (ANOVA) at 5% significance, followed by comparison of means using Tukey's test ($p \leq 0.05$). When the interaction between factors was significant, we conducted *post hoc* analyses to interpret the results more precisely.

Image acquisition and processing

Hyperspectral images were captured with a Headwall Nano-Hyperspec® (Headwall Photonics, USA) CMOS sensor mounted to a DJI Ronin gimbal stabilizer on a DJI MATRICE™ M600Pro six-rotor drone. This sensor uses a pushbroom scanning approach, acquiring 640 spatial pixels and 271 spectral bands, resulting in 173,440 spatial-spectral data points per line. Additionally, the 12-bit sensor identifies 4,096 brightness levels from 400 to 1000 nm, covering the entire visible and near-infrared (NIR) spectrum, with 2.2 nm intervals and a half bandwidth of approximately 6 nm.

Imaging was captured twice in 2022, and three times in 2023, before and after symptom onset. The flights were conducted at 80 m altitude at 6 and 23 DAI (V3 and V4 phenological stages, respectively) in 2022, and at 8, 10 (V3), and 22 DAI (V4) in 2023. Radiometric calibration was performed to ensure that the images accurately represent surface reflectance (Suomalainen et al., 2021). Images were then orthorectified and converted into reflectance using the Headwall's SpectralView software. After image processing, data and .tiff files containing reflectance for each image pixel were generated. Using QGIS software (qgis.org), a shapefile layer was created. Twelve random points corresponding to the leaf area of the common bean plants in the image were marked. Then, the GDAL (Geospatial Data Abstraction Library) library (GDAL/OGR contributors, 2024) was used with Python, edited in Visual Studio Code (version 1.76.2), to obtain the corresponding reflectance data.

Reflectance analysis

The analysis of reflectance data recorded with hyperspectral imaging was based on comparing linear and mixed-effects model structures. Four models were fitted to the data: (1) an interactive mixed linear model, (2) an additive mixed linear model, (3) an interactive linear model, and (4) an additive linear model (Bates et al., 2015). In all models, inoculation, straw mulch, and common bean cultivar were included as fixed effects, whereas the experimental blocks were modeled as a random effect. The competing models were compared using likelihood ratio tests between nested specifications fitted by maximum likelihood, and the one with best balance between goodness of fit and parsimony was selected as the final model.

Model assumptions were evaluated through visual inspection of residual diagnostics, including residuals vs fitted plots and the Goldfeld-Quandt test for heteroscedasticity. An exploratory analysis was conducted to select the variables (spectral bands) that best fit the proposed model at 5% significance level, using the coefficients of determination (R^2), the Akaike Information Criterion (AIC), and the Sum of Squares of Errors (SSE). We sought to establish coherence among these three criteria and to select spectral bands that remained consistent across the criteria, prioritizing significance and higher-order metrics (R^2) over lower-order metrics (AIC and SSE). This approach aims to ensure a consistent assessment of the variables considered in the study (Alves et al., 2019). Once these requirements were met and the model chosen, the regression models that best explained the relationships between the dependent and the independent variables were compared using the likelihood ratio test. All linear and mixed-effects models were fitted in R 4.3.2 (R Core Team, 2025) using base functionality (lm and associated functions).

Results

Disease severity

In 2022, the disease progress was evident in the BRS FC401 RMD cultivar. Typical symptoms of CPMMV were observed, including chlorosis advancing from light in young plants to severe in late phenological stages, along with mottling and leaf deformation, and higher DSI was observed in bare-soil plots (Fig. 1). The BRS FC420 RMD cultivar had a different response to infection. Although the first symptoms were also light chlorosis and mottling, new shoots and leaves produced after the V4 stage were almost asymptomatic and difficult to detect visually later, supporting the cultivar's CPMMV-tolerant status (Silva et al 2022). The DSI progress curves for the susceptible cultivar showed a moderate adjustment, with R^2 values of 0.76 and 0.69 in bare and mulched soil, respectively. Disease progress in the BRS FC420 RMD cultivar grown in plots with bare soil could was fit by a linear model with $R^2 = 0.74$. In contrast, the CPMMV progress in this cultivar on plots with mulch had a poor fit ($R^2 = 0.48$).

Despite standard inoculation and disease assessment procedures and overall crop management, plants of both cultivars showed more severe viral infection symptoms in 2023. This year, disease progress was more pronounced in both cultivars. Again, BRS FC401 RMD showed higher DSI in soil-covered plots, whether with or without mulch, and mottling and severe leaf deformation were more frequent. The DSI was higher than in 2022 for the susceptible cultivar BRS FC401 RMD, especially in bare-soil plots. The higher frequency of infected plants with more severe symptoms likely improved the fit of the DSI × time model, with $R^2 \geq 0.90$ in all cases. Regarding the BRS FC420 RMD cultivar, higher DSI levels did not prevent the release of asymptomatic leaves or the appearance of light symptoms as plants approached the blooming stage, and DSI remained almost stable from June 23 onward.

In the CPMMV plots, all plants were inoculated individually, so it was expected that all would develop CPMMV infection. CPMMV infection in the two common bean genotypes was confirmed by molecular analysis. In some mechanically inoculated plots, CPMMV was not detected on the first sampling date (about 12 DAI) in both years (Table 1), whereas it was detected by hyperspectral imaging at 6 and 8 DAI. However, when new samples were collected later (at 34 DAI in 2022 and 28 DAI in 2023), all inoculated plots were symptomatic and tested positive for CPMMV, except one plot with the tolerant cultivar BRS FC420 RMD in 2022. As shown by the DSI progress curves (Figure 1), CPMMV infection did not develop well in the plants of the tolerant cultivar. The plots not inoculated (controls) were also sampled, and all samples tested negative for CPMMV (data not shown). The absence of whiteflies prevented plant infection in the control plots.

Table 1 Detection of *Carlavirus vignae* (CPMMV) in common bean plants of the cultivars BRS FC401 RMD and BRS FC420 RMD by RT-PCR at 12 and 34 days (2022) and 12 and 28 days (2023) after mechanical inoculation (DAI) in field experiments conducted in 2022 and 2023.

Year	DAI	Cultivars	RT-PCR Positive (+) / Total
2022	12	BRS FC401 RMD	9/10
		BRS FC420 RMD	5/10
	34	BRS FC401 RMD	10/10
		BRS FC420 RMD	9/10
2023	12	BRS FC401 RMD	9/10
		BRS FC420 RMD	10/10
	28	BRS FC401 RMD	10/10
		BRS FC420 RMD	10/10

3.2 Crop yield and yield components

Considering the average of the 2022 and 2023 experiments, the common bean yield was significantly higher (~21.6%) in the non-inoculated plots (2478.2 kg ha^{-1}) than in the inoculated plots (Fig. 2A). When comparing the two cultivars, non-inoculated plants were more productive than infected plants, as indicated by yield and 100-grain weight (Figs. 2B and 2C). The average yield of the tolerant cultivar BRS FC420 RMD did not differ from that of the susceptible BRS FC401 RMD, possibly because the former has a semi-upright growth habit with fewer nodes for pod formation than the latter, which has a prostate, branched growth habit.

3.3 Hyperspectral response

Plant canopy reflectance was significantly affected by CPMMV inoculation in both years of the field experiment (Table 2). To identify the wavelengths most strongly associated with the response variables, candidate regression models were fitted separately for each of the 271 wavelengths. Based on the p-values, lowest SSE, AIC and the highest R^2, the wavelengths were ranked to identify those with the strongest association with the independent variables. In all imaging flights conducted in 2022 and 2033, whether with asymptomatic or symptomatic plants, linear additive models provided the best fit to explain differences between infected and healthy plants. The optimal bands at 414.8, 401.6, 417.0, 425.9 and 421.4 nm were selected because they simultaneously yielded the highest R^2 and the lowest AIC and SSE indices for the imaging flights at 6 and 22 DAI in 2022, and at 8, 10 and 23 DAI in 2023, respectively. All possible interactions were tested in the candidate models, but none provided evidence of effect modification; therefore, the final models were retained without interaction terms.

The spectral bands that best fit the reflectance × predictor variables (inoculation, soil cover) had a half-bandwidth of 25 nm between 401 nm and ~426 nm (Fig. 3). Comparing early- and late-flights within the same year, fit statistics were higher when reflectance was assessed at the V3 phenological stage of common beans, when inoculated plants were still asymptomatic. R^2 values for flights conducted between 8 and 11 DAI ranged from 0.74 to 0.78, whereas lower values (~0.62) were observed at 22–23 DAI, regardless of the experimental year.

Table 2. Fit statistics and parameter estimates for the additive linear models adjusted to describe the hyperspectral response of BRS FC401 RMD plants inoculated with CPMMV in 2022 and 2023. Model selection was based on the coefficient of determination (R^2), Akaike information criterion (AIC), and sum of squared errors (SSE).

DAI	Band (nm)	R^2	AIC	SSE	Parameter	Estimate	Std. Error	t value	P-value
6	414.8	0.78	-277.5857	0.0001824206	Intercept	0.00550122	0.0020421	26.94	<0.001
					Cultivar	0.0045295	0.0011812	3.835	0.006
					Inoculation	-00.21228	0.0011889	-1.785	0.0854
					Soil cover	-0.0051699	0.0011889	-4.348	0.0002
8	417.0	0.73	-642.4603	$3.269221e^{-05}$	Intercept	$6.41e^{-03}$	$2.65e^{-04}$	24.202	<0.001
					Cultivar	$4.69e^{-04}$	$1.84e^{-04}$	2.543	0.0135
					Inoculation	$-1.68e^{-03}$	$1.85e^{-04}$	-9.057	<0.001
					Soil cover	$-1.23e^{-03}$	$1.86e^{-04}$	-6.621	<0.001
10	425.9	0.79	-863.6378	$6.934322e^{-05}$	Intercept	$1.11e^{-02}$	$3.21e^{-04}$	34.535	<0.001
					Cultivar	$1.34e^{-03}$	$2.21e^{-04}$	6.09	<0.001
					Inoculation	$-2.17e^{-03}$	$2.21e^{-04}$	-9.829	<0.001
					Soil cover	$-2.54e^{-03}$	$2.21e^{-04}$	-11.509	<0.001
22	401.6	0.62	-331.6640	$2.114725e^{-05}$	Intercept	$3.66e^{-03}$	$4.11e^{-04}$	8.903	<0.001
					Cultivar	$6.76e^{-05}$	$2.82e^{-04}$	0.24	0.812
					Inoculation	$-1.31e^{-04}$	$2.82e^{-04}$	-4.657	<0.0001
					Soil cover	$-3,98e^{-04}$	$2.82e^{-04}$	-1.414	0.166
23	421.4	0.64	-526.4765	$1.560154e^{-06}$	Intercept	$3.55e^{-03}$	$1.04e^{-04}$	34.283	<0.0001
					Cultivar	$-2.71e^{-05}$	$7.09e^{-05}$	-0.382	0.70459
					Inoculation	$-3.06e^{-04}$	$7.06e^{-05}$	-4.337	0.0001
					Soil cover	$-4.08e^{-04}$	$7.06e^{-05}$	-5.779	<0.0001

Reflectance differences among common bean cultivars varied with plant age and year, with cultivars distinguishable at some stages but not at others. Still, the central wavelength near 415 nm consistently distinguished BRS FC401 RMD from BRS FC420 RMD plants when they had no CPMMV symptoms at the V3 stage. Both cultivars could not be distinguished by their reflectance at later assessments. This outcome provides further evidence that cultivar discrimination diminishes at later stages, reinforcing the importance of linking early-stage results (6–8 DAI) to state-of-the-art literature on physiological changes following infection.

Soil mulch with grass straw affected reflectance assessments at 5% significance in all flights, in the visible light spectrum regions corresponding to *circa* 400-520 nm and 580-700 nm. In all other hyperspectral imaging flights during 2023 and at 6 DAI in 2022, the soil cover affected canopy reflectance (Fig. 4). Further, reflectance was affected by soil cover in the near-infrared region (~720-1000 nm) in all flights, except at 22 DAI in 2022.

Discussion

Two years of field testing demonstrated that remote sensing using hyperspectral imaging can detect the early stages of CPMMV infection in common beans. Timely action is crucial for limiting the spread of viruses in annual crops, because effective control depends on preventive measures and the accurate timing of interventions (Anikina et al., 2023). Diagnosing viral infections in plants, such as CPMMV in common beans, is generally done once symptoms are apparent and the virus is established in the plant. At this point, controlling the spread of the virus is challenging because infected plants may already have been a source of new infections when whiteflies are present in the field, especially for viruses transmitted in a non-circulative mode.

Infected plants exhibit distinct reflectance patterns, especially in the 400-425 nm band, which corresponds to the blue-light absorption by chlorophyll a (Falcioni et al., 2023). Such changes suggest chlorophyll degradation and stress of the photosynthetic apparatus, which were detectable even before symptom onset. The best discrimination band (~415 to 425 nm) for early detection of CPMMV falls in the blue absorption region of chlorophyll a, where infection-induced chlorophyll degradation and pheophytinization alter canopy reflectance. This aligns with reports that 415 nm is highly informative for early infection or stress in other pathosystems, notably *Xylella fastidiosa* in olive (Zarco-Tejada et al., 2018), but different from virus detection in vines (VIS and red-edge bands at 400–700 nm) (Nguyen et al., 2021) and tobacco (510–630 nm and 690–720 nm) (Grishina et al., 2023).

In this study, we present the initial hyperspectral plant response parameters of common bean plants infected with CPMMV to select wavelengths that can serve as a digital signature, i.e., indicators of the virus's presence even at an initial stage of infection. Analysis of reflectance variations across visible and near infrared spectral bands identified specific wavelengths associated with the virus at the early and late stages of infection. Early detection of CPMMV with hyperspectral imaging is possible, corroborating findings from other studies on plant viruses (Gu et al., 2019). Indeed, the detection of CPMMV-infected plants using reflectance data was confirmed by RT-PCR (Table 2), despite the effects of soil cover and the different reactions of the two common bean genotypes.

Both bare soil and mulch established by cover crops exhibit distinct background optical properties and may affect plant canopy reflectance; the differences reported here are consistent with those of Gao et al. (2022). Although CPMMV symptoms developed on the upper canopy and remained visually apparent (not shaded), the specific row spacing and plant arrangement used here (narrow rows with reduced plants per row but unchanged plant density per m²) may still have influenced canopy architecture and background contributions, potentially modulating the spectral separation between inoculated and non-inoculated plots. We also consider that soil cover was decisive in affecting reflectance. Still, it may have affected other sources of variation besides the plant’s response to infection, such as soil moisture and root colonization by soilborne microorganisms. Therefore, changes in background conditions may influence spectral responses, indicating that future algorithm development should account for these sources of variability to ensure robust detection.

The selected bands that best fit the parameters used to identify CPMMV infection in both cultivars were within a narrow range of the visible electromagnetic spectrum, from 400 to 425 nm, during flights at the pre-symptomatic and symptomatic stages. The bands that best fit the parameters for each date varied little among cultivars and crop phenological stage, particularly at the initial stage of infection. At early stages (6, 8, and 10 DAI), reflectance differences between inoculated and control plants were most pronounced in the 414.8–425.9 nm spectral range. At later stages (22–23 DAI), differences were primarily observed between 401.6 and 421.4 nm.

Differences in DSI progress curves confirmed the observed variations between cultivars. While the virus developed more severe symptoms in the susceptible cultivar, which was more evident in 2022 than in 2023, the tolerant cultivar presented, at most, mild symptoms. Consistently, the BRS FC420 RMD DSI progress curves reported in both years of field testing were lower than in the susceptible genotype. This result indicated that, although a short interval of spectral bands can be used to identify plant CPMMV infections, further differences among common bean genotypes, virus inoculation and soil

cover in wider bandwidths (e.g., 400 - 700 nm) indicated that, possibly, multispectral sensors may also be used to identify viral infections.

The CPMMV DSI in the tolerant cultivar was lower during the blooming and pod filling stages, possibly because, as the plants grew, newly developed leaves were less affected by virus replication than the older leaves formed right after inoculation (Silva et al., 2022). Indeed, the DSI curves for the BRS FC420 RMD cultivar were diminished as the plants aged, supporting its tolerance. It is known that viral diseases are more severe and yield penalties are greater when plants are infected at early developmental stages (Mar et al., 2017).

In commercial fields, when whiteflies transmit CPMMV, there is normally a mix of healthy and infected plants in different proportions that rapidly expands as the vector population grows (Morales & Jones, 2004; Ferreira et al., 2024), particularly under high plant density and conducive weather conditions. In this case, diagnosing young plants, even if some are already symptomatic, still underscores the need to advise control measures and protect healthy seedlings. Remote sensing routines with hyperspectral sensors could, in this case, provide a gain of several days in detecting CPMMV infections and triggering control measures that mitigate yield losses.

The spread of viruses depends on the effectiveness of the inoculum source, the presence of insect vectors and the plant host reaction. Although mechanical inoculation of the BRS FC420 RMD cultivar resulted in no more than light symptoms (Silva et al. 2022), its tolerance mechanism has not yet been described. Our results suggest that the physiological responses of this common bean genotype to CPMMV are active a few days after virus inoculation. Furthermore, our results also showed that CPMMV infection significantly reduced common bean yield up to 21%, underscoring the impact of this virus on common bean production and the importance of developing more efficient tools for field virus monitoring and tolerant genotypes.

Scouting reflectance of common beans may inform stakeholders in advance, enabling management of CPMMV and supporting the implementation of precision agriculture strategies that optimize insecticide applications for vector management. We concluded that differences in plant canopy reflectance in the short interval of the visible electromagnetic spectrum from 400 to 425 nm can be used to detect *C. vignae* infection in common beans. Soil cover affects common bean reflectance and the detection of the virus at early stages. These findings can be used to validate the detection method using hyperspectral sensors in commercial fields and to improve IPM and decision-making, thereby significantly contributing to disease management.

Declarations

FUNDING

This work was funded by Embrapa (grant 20.19.03.057.00) and the National Council for Scientific and Technological Development (CNPq grant 400574/2022-5). The authors are grateful to the Coordination for the Improvement of Higher Education Personnel (CAPES) and to FAPEG (Foundation for Research Support of Goiás State) for awarding graduate scholarships to William Rafael Ribeiro, Amanda Lopes Ferreira, and Andressa de Souza Almeida. This research study was supported by the Brazilian Ministry of Environment (SISGEN authorization AADB536).

AUTHOR'S CONTRIBUTIONS

Conceptualization: MLJ, TMA, AMG, PVP; methodology: WRR, JFAS, ASA, RMS, TMA, AMG, PVP, MLJ; data curation: PVP, MLJ, investigation: WRR, JFAS, ASA, RMS, TMA, AMG, PVP, MLJ; formal analysis: WRR, JFAS, ASA, RMS, TMA, AMG, PVP, MLJ; writing – original draft: WRR, JFAS, TMA, AMG, PVP, MLJ; funding acquisition: MLJ; supervision, review & editing: TMA, AMG, PVP, MLJ.

CONFLICT OF INTEREST STATEMENT

The authors declare that they have no competing, financial or personal interests of any nature in this paper.

DATA AVAILABILITY STATEMENT

The experimental data of this study will be available upon reasonable request.

ORCID

William Rafael Ribeiro https://orcid.org/0000-0003-0213-8129

José Francisco Arruda e Silva https://orcid.org/0000-0002-0604-8174

Andressa de Souza Almeida https://orcid.org/0000-0002-5225-7882

Amanda Lopes Ferreira https://orcid.org/0009-0008-4841-871X

Rômulo Moreira Silva https://orcid.org/0000-0001-5060-8493

Tavvs Micael Alves https://orcid.org/0000-0002-4660-9191

Alaerson Maia Geraldine https://orcid.org/0000-0001-6794-9665

Patrícia Valle Pinheiro https://orcid.org/0000-0003-0461-1821

Murillo Lobo Junior https://orcid.org/0000-0002-3681-4570

References

1. Alves TM, Macrae IV, Koch RL. 2015. Soybean Aphid (Hemiptera: Aphididae) Affects Soybean Spectral Reflectance. J. Econ. Entomol. 108:2655–2664. doi:10.1093/jee/tov250.
2. Alves TM, Moon RD, MacRae IV, Koch RL. 2019. Optimizing band selection for spectral detection of *Aphis glycines* Matsumura in soybean. Pest Man. Sci. 75:942–949. https://doi.org/10.1002/ps.5198
3. Alves-Freitas DMT, Pinheiro-Lima B, Faria JC, Lacorte C, Ribeiro SG, Melo FL. Double-Stranded RNA High-Throughput Sequencing Reveals a New Cytorhabdovirus in a Bean Golden Mosaic Virus-Resistant Common Bean Transgenic Line. Viruses. 2019 Jan 21;11(1):90. doi: 10.3390/v11010090. 02/ps. 5198.
4. Anikina I, Kamarova A, Issayeva K, Issakhanova S, Mustafayeva N, Insebayeva M, Mukhamedzhanova A, Khan SM, Ahmad Z, Lho LH, Han H, Raposo A. (2023). Plant protection from virus: a review of different approaches. Front Plant Sci. 12:1163270. doi: 10.3389/fpls.2023.1163270.
5. Bates, D., Mächler, M., Bolker, B., & Walker, S. 2015. Fitting Linear Mixed-Effects Models Using lme4. Journal of Statistical Software, 67: 1–48. https://doi.org/10.18637/jss.v067.i01
6. Bock, C.H., Barbedo, J.G.A., Del Ponte, E.M. et al. 2020. From visual estimates to fully automated sensor-based measurements of plant disease severity: status and challenges for improving accuracy. Phytopathol. Res. 2:9. https://doi.org/10.1186/s42483-020-00049-8
7. Chiang, K-S.; Liu, H. I.; Bock, C. H. 2017. A discussion on disease severity index values: I. Warning on inherent errors and suggestions to maximize accuracy. Ann. Appl. Biol. 171:139–154. https://doi.org/10.1111/aab.12362.
8. Devadas, R.; Lamb, D. W.; Simpfendorfer, S.; Backhouse, D. 2009. Evaluating ten spectral vegetation indices for identifying rust infection in individual wheat leaves. Precis. Agric. 10:459–470. https://doi.org/10.1007/s11119-008-9100-2.

9. Falcioni, R., Antunes, W. C., Demattê, J. A. M., Nanni, M. R. (2023). A Novel Method for Estimating Chlorophyll and Carotenoid Concentrations in Leaves: A Two Hyperspectral Sensor Approach. Sensors, 23(8), 3843. https://doi.org/10.3390/s23083843
10. Faria, J.; Aragão, F. J. L.; Souza, T. L. P. O.; Quintela, E. D.; Kitajima, E. W.; Ribeiro, S. G. 2016. Golden mosaic of common beans in Brazil: management with a transgenic approach. APS Features 10. doi:10.1094/APSFeature-2016-10.
11. Ferreira A. L., Ghanim M., Xu Y., Pinheiro P. V. (2024). Interactions between Common Bean Viruses and Their Whitefly Vector. Viruses 16:1567. doi: 10.3390/v16101567.
12. Gao L., Darvishzadeh R., Somers B., Johnson B.A., Wang Y., Verrelst J., Wang X., Atzberger C. (2022). Hyperspectral response of agronomic variables to background optical variability: Results of a numerical experiment. Agric For Meteorol. 326:109178. doi: 10.1016/j.agrformet.2022.109178.
13. GDAL/OGR contributors. 2024. GDAL/OGR Geospatial Data Abstraction Software Library. Open Source Geospatial Foundation. URL https://gdal.org. DOI: 10.5281/zenodo.5884351.
14. Gold, K. M.; Townsend, P. A.; Chlus, A.; Couture, J. J.; Herrmann, I.; Larson, E. R; Gevens, A. J. 2020. Hyperspectral measurements enable pre-symptomatic detection and differentiation of contrasting physiological effects of late blight and early blight in potato. Remote Sens. 12, 286. https://doi.org/10.3390/rs12020286.
15. Grishina, A., Sherstneva, O., Zhavoronkova, A., Ageyeva, M., Zdobnova, T., Lysov, M., Brilkina, A., & Vodeneev, V. (2023). Comparison of the Efficiency of Hyperspectral and Pulse Amplitude Modulation Imaging Methods in Pre-Symptomatic Virus Detection in Tobacco Plants. Plants, 12, 3831. https://doi.org/10.3390/plants12223831
16. Gu, Q.; Sheng, L.; Zhang, T.; Lu, Y.; Zhang, Z.; Zheng, K.; Hu, H.; Zhou, H. 2019. Early detection of tomato spotted wilt virus infection in tobacco using the hyperspectral imaging technique and machine learning algorithms. Comput. Electron. Agric. 167: 105066. doi:10.1016/j.compag.2019.105066.
17. Lamas N.S .; Matos, V. O. R. L.; Alves-Freitas, D. M. T.; Melo, F. L.; Costa, A. F.; Faria, J. C.; Ribeiro, S. G. 2017. Occurrence of *Cowpea mild mottle virus* in Common Bean and Associated Weeds in Northeastern Brazil. Plant Dis. 101:1828–1828. doi:10.1094/PDIS-04-17-0562-PDN.
18. Lowe, A.; Harrison, N.; French, A. P. 2017. Hyperspectral image analysis techniques for the detection and classification of the early onset of plant disease and stress. Plant Methods. 13:80. doi:10.1186/s13007-017-0233-z.
19. Luo, L.; Chang, Q.; Wang, Q.; Huang, Y. 2021. Identification and Severity Monitoring of Maize Dwarf Mosaic Virus Infection Based on Hyperspectral Measurements. Remote Sens. 13:4560. doi:10.3390/rs13224560.
20. Mahlein, A. K. 2016. Plant Disease Detection by Imaging Sensors – Parallels and Specific Demands for Precision Agriculture and Plant Phenotyping. Plant Dis. 100: 241-251. https://doi.org/10.1094/PDIS-03-15-0340-FE.
21. Mahlein, A.-K., Kuska, M.T., Behmann, J., Polder, G., Walter, A. 2018. Hyperspectral Sensors and Imaging Technologies in Phytopathology: State of the Art. Annu. Rev. Phytopathol., 56:535-558. https://doi.org/10.1146/annurev-phyto-080417-050100.
22. Mar, T. B.; Mendes, I. R.; Lau, D.; Fiallo-Olivé, E.; Navas-Castillo, J.; Alves, M. S.; Zerbini, F. M. 2017. Interaction between the New World begomovirus *Euphorbia yellow mosaic virus* and its associated alphasatellite: effects on infection and transmission by the whitefly *Bemisia tabaci*. J. Gen. Virol. 98:1552–1562. https://doi.org/10.1099/jgv.0.000814.
23. Morales FJ, Jones PG. (2004). The ecology and epidemiology of whitefly-transmitted viruses in Latin America. Virus Res. Mar, 100:57-65. doi: 10.1016/j.virusres.2003.12.014.
24. Nguyen, C.; Sagan, V.; Maimaitiyiming, M.; Maimaitijiang, M.; Bhadra, S.; Kwasniewski, M. T. 2021. Early Detection of Plant Viral Disease Using Hyperspectral Imaging and Deep Learning. Sensors, 21:742. https://doi.org/10.3390/s21030742
25. Paudel, S.; Bechinski, E. J.; Stokes, B.S.; Pappu, H.R.; Eigenbrode, S.D. 2018. Deriving Economic Models for Pea Aphid (Hemiptera: Aphididae) as a Direct-Pest and a Virus-Vector on Commercial Lentils. J. Econ. Entomol. 111:2225–

2232. https://doi.org/10.1093/jee/toy188.

26. R Core Team R. 2022. A Language and Environment for Statistical Computing. R Foundation for Statistical Computing, Vienna, Austria. https://www.R-project.org/, "R version 4.2.2 (2024-10-31).
27. Silva, R. S.; Faria J. C.; Knupp, A. M.; Aguiar, M. S.; Pereira, H. S.; Ferreira, A. L.; Zaidem, A. L. M.; Pinheiro, P. V.; Melo, L. C.; Souza, T. L. P. O. 2022. Development and selection of transgenic advanced lines of carioca seeded common bean with multiple resistance to viruses. Euphytica. 218:67. doi:10.1007/s10681-022-03017-9.
28. Silva, R. S.; Faria, J. C.; Vianello, R. P.; Valdisser, P. A. M. R.; Pereira, H. S.; Melo, L. C.; Pinheiro, P. V.; Souza, T. L. P. O. 2024. Inheritance and genetic mapping of the first CPMMV tolerance locus in common bean. Plant Pathol. 73:1436–1445. doi:10.1111/ppa.13892. https://doi.org/10.1111/ppa.13892.
29. Souza, T. L. P. O.; Faria, J. C.; Aragão, F. J. L.; Del Peloso, M. J.; Faria, L. C.; Aguiar, M. S.; Wendland, A.; Quintela, E. D.; Diaz, J. L. C.; Magaldi, M. et al. 2016. BRS FC401 RMD: cultivar de feijão carioca geneticamente modificada com resistência ao mosaico-dourado. https://ainfo.cnptia.embrapa.br/digital/bitstream/item/149329/1/CNPAF-2016-ct235.pdf.
30. Suomalainen, J.; Oliveira, R. A.; Hakala, T.; Koivumäki, N.; Markelin, L.; Näsi, R.; Honkavaara, E. 2021. Direct reflectance transformation methodology for drone-based hyperspectral imaging. Remote Sens. Environ. 266:112691. https://doi.org/10.1016/j.rse.2021.112691.
31. Terentev, A.; Dolzhenko, V.; Fedotov, A.; Eremenko, D. 2022. Current State of Hyperspectral Remote Sensing for Early Plant Disease Detection: A Review. Sensors, 22:757. https://doi.org/10.3390/s22030757
32. Tucker, C. J. 1979. Red and photographic infrared linear combinations for monitoring vegetation. Remote Sens. Environ. 8:127–150. https://doi.org/10.1016/0034-4257(79)90013-0.
33. Zanardo, L. G.; Carvalho, C. M. 2017. *Cowpea mild mottle virus* (Carlavirus, Betaflexiviridae): a review. Trop. Plant Pathol. 42:417–430. https://doi.org/10.1007/s40858-017-0168-y.
34. Zarco-Tejada PJ, Camino C, Beck PSA, Calderon R, Hornero A, Hernández-Clemente R, Kattenborn T, Montes-Borrego M, Susca L, Morelli M, Gonzalez-Dugo V, North PRJ, Landa BB, Boscia D, Saponari M, Navas-Cortes JA. 2018. Previsual symptoms of *Xylella fastidiosa* infection revealed in spectral plant-trait alterations. Nat Plants. 4: 432-439. doi: 10.1038/s41477-018-0189-7.
35. Zhang, J.; Huang, Y.; Pu, R.; Gonzalez-Moreno, P.; Yuan, L.; Wu, K.; Huang, W. 2019. Monitoring plant diseases and pests through remote sensing technology: A review. Comput. Electron. Agric. 165:104943. https://doi.org/10.1016/j.compag.2019.104943.

Figures

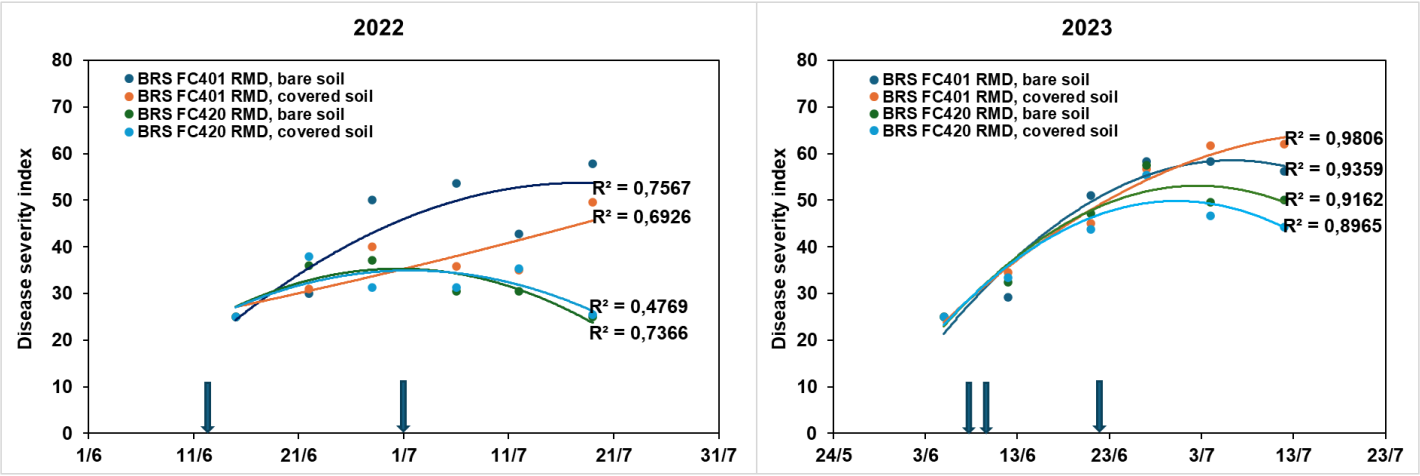


Figure 1

Disease severity index progress curves of *Carlavirus vignae* (CPMMV) in the BRS FC401 RMD and BRS FC420 RMD common bean cultivars, with respective coefficients of determination in 2022 and 2023. Arrows indicate the day of flights for hyperspectral imaging.

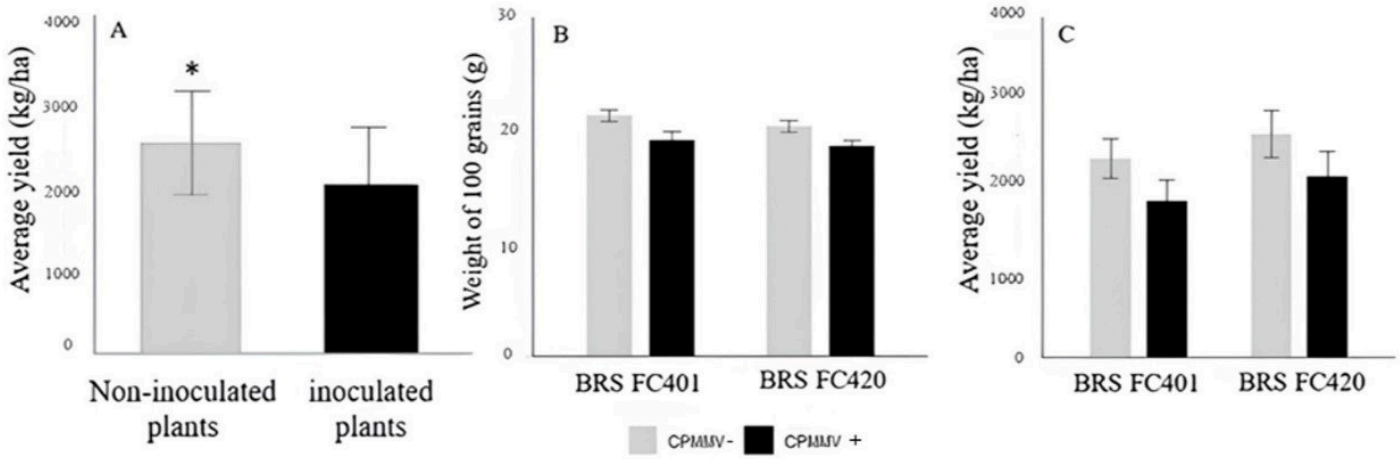


Figure 2

Average common bean yield in the 2022–2023 experiments. (A) Mean yield of the two cultivars, BRS FC401 RMD and BRS FC420 RMD, considering inoculated and non-inoculated plants together (p=0.00215). (B) Mean yield of inoculated and non-inoculated plants within each cultivar. (C) Mean 100-grain mass of inoculated and non-inoculated plants within each cultivar.

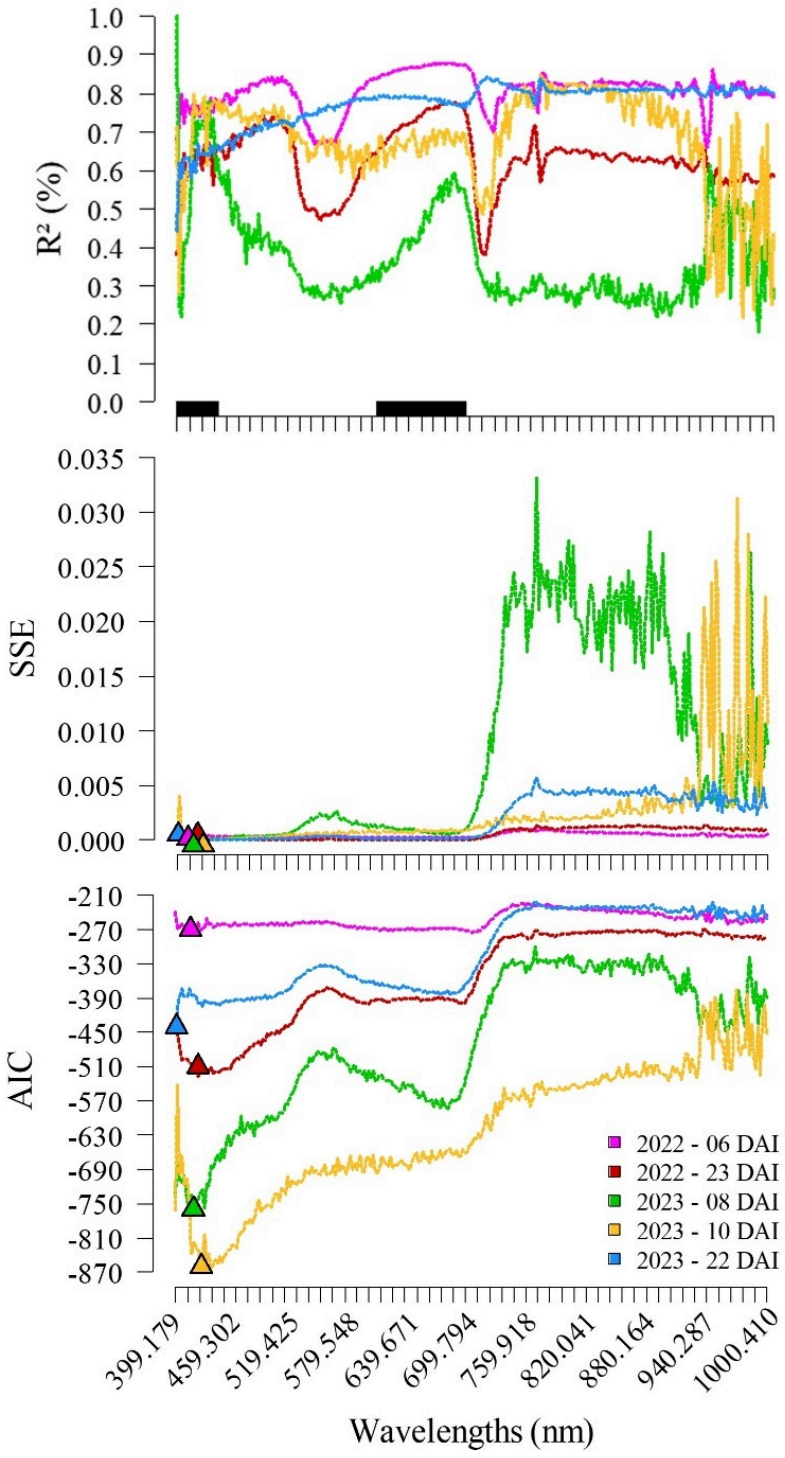


Figure 3

Results of regression models fitting to evaluate *Carlavirus vignae* (CPMMV) infection in common bean genotypes based on hyperspectral imaging across the 400–1000 nm spectral range. Model selection was based on the coefficient of determination (R^2), sum of squared errors (SSE), and Akaike information criterion (AIC). Dark boxes indicate wavelengths with significant p-values. Colored triangles indicate reflectances in the 400–425 nm region that better represented the differences between infected and healthy plants at 6 and 23 days after inoculation (DAI) in 2022 and at 8, 11, and 22 DAI in 2023.

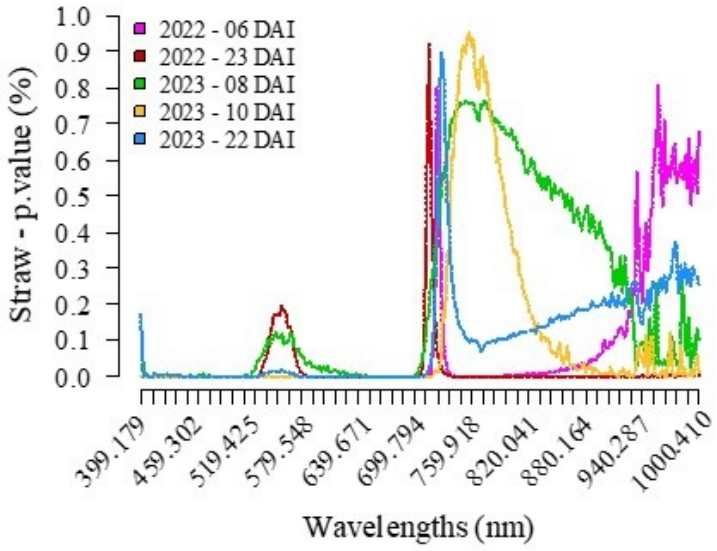


Figure 4

P-values from linear regression models fitted to assess the association between *Carlavirus vignae* (CPMMV) inoculation and common bean reflectance across 271 wavelengths from 400 to 1000 nm. The figure summarizes results from field experiments conducted in 2022 and 2023, highlighting the wavelengths at which reflectance differed significantly between plots with mulch and bare soil. DAI = days after inoculation.